Critical crossover phenomena driven by symmetry-breaking defects at quantum transitions

Alessio Franchi ⬤, Davide Rossini ⬤, and Ettore Vicari*

Dipartimento di Fisica dell'Università di Pisa and INFN, Largo Pontecorvo 3, I-56127 Pisa, Italy

We study the effects of symmetry-breaking defects at continuous quantum transitions (CQTs) of homogeneous systems, which may arise from localized external fields coupled to the order-parameter operator. The problem is addressed within renormalization-group (RG) and finite-size scaling frameworks. We consider the paradigmatic one-dimensional quantum Ising models at their CQT, in the presence of defects which break the global $\mathbb{Z}_2$ symmetry. We show that such defects can give rise to notable critical crossover regimes where the ground-state properties experience substantial and rapid changes, from symmetric conditions to characterization of these crossover phenomena driven by defects. In particular, this is demonstrated by analyzing the ground-state fidelity associated with small changes of the defect strength. Within the critical crossover regime, the fidelity susceptibility shows a power-law divergence when increasing the system size, related to the RG dimension of the defect strength; in contrast, outside the critical defect regime, it remains finite. We support the RG scaling arguments with numerical results.

I. INTRODUCTION

Critical phenomena have attracted much interest in recent decades (see, e.g., Refs. [1–10] and references therein). One of the reasons is that their emerging features have a great degree of universality, being largely independent of the microscopic details. Therefore they have a wide applicability to different systems and within very different physical contexts. Moreover, they allow us to describe complex phenomena using a relatively small number of relevant variables, providing a notable simplification of the analysis of many-body systems. However, critical phenomena occur under particular conditions, when the system develops long-range correlations, for example, at continuous phase transitions arising from thermal or quantum fluctuations.

Some important features of critical phenomena at thermal and quantum continuous phase transitions are related to the presence of boundaries [11–17] and the presence of defects [18–28]. These are not academic issues, since physical systems generally have boundaries and are subject to localized defects of various nature. The presence of isolated defects does not generally change the bulk power-law behaviors characterizing the critical behavior of observables at large scale. However, their effects may get somehow amplified by the long-range critical modes at continuous transitions, in the neighborhood of the defect, and in particular in finite-size systems. Symmetry-preserving bond defects have been mostly investigated in the literature, in both classical and quantum systems (see, e.g., Refs. [18–20,23,26,27]). We mention that

the local magnetization along a line of symmetry-preserving bond defects develops a peculiar behavior in classical systems, being characterized by the continuous variation of its critical exponent when varying the strength of the bond defects [18–20]. In contrast, here we focus on defects of different nature, i.e., those that break the global symmetry within homogeneous systems.

In this paper we investigate the effects of symmetry-breaking defects in quantum many-body systems at continuous quantum transitions (CQTs). We address these issues exploiting renormalization-group (RG) and finite-size scaling (FSS) frameworks. We argue that, although the presence of isolated defects does not generally change the bulk power-law behaviors at CQTs, they can drive notable critical crossover behaviors when the defects are the only source of symmetry breaking in homogeneous systems. In this case they induce critical crossovers in the ground-state and low-energy properties, between limiting cases that can be associated with different boundary conditions: from boundary conditions (or absence of boundaries) preserving the global symmetry to boundary conditions breaking the symmetry associated with the CQT. Therefore, the addition of isolated symmetry-breaking defects to critical (strictly symmetric) systems can give rise to substantial changes of the ground states and the finite-size behavior of the critical modes, even in the large-size limit within the FSS regime around the CQT. Two different situations, which develop different RG properties, must be distinguished: whether the defects are located within the bulk of the system, or at the boundaries.

We challenge this general scenario within the paradigmatic one-dimensional quantum Ising systems in a transverse field, studying the effects of local defects breaking the global $\mathbb{Z}_2$ symmetry, within the bulk and at the boundaries. We analyze the crossover behaviors induced by the defects at its CQT

---

when varying their strength. These critical defect crossovers provide a bridge between situations that can be associated with different boundary conditions: from translation-invariant FSS behaviors in Ising rings to FSS behaviors of systems with parallel fixed boundary conditions (PFBC). The power laws characterizing these critical crossovers are determined by the RG dimensions of the perturbations arising from the defects, which differ for defects within the bulk and at the boundaries. The scaling theory that we develop is then checked by numerical computations.

An effective characterization of the crossover phenomena driven by symmetry-breaking defects is obtained by analyzing the ground-state fidelity measuring the overlap between ground states associated with different defect parameters. This provides information on the variations of the ground-state structures due to the defect, whether it gives rise to substantial changes involving the whole system, or the changes remain limited to a finite region. We argue that the susceptibility associated with the defect fidelity diverges in the large-size limit within the critical crossover regime, while it remains finite outside it. Such a power-law divergence is related to the RG dimension of the defect parameter.

The paper is organized as follows. In Sec. II we introduce the models that we consider, i.e., quantum Ising rings without boundaries [corresponding to periodic boundary conditions (PBC)] in the presence of one symmetry-breaking defect, and Ising chains with boundaries [such as open boundary conditions (OBC)] with defects localized at the boundaries. In Sec. III we introduce the quantities that we use to monitor the effects of the symmetry-breaking defects, including the ground-state fidelity associated with small changes of the defect parameters. In Sec. IV we outline the description of the critical defect crossover phenomena in Ising rings, using RG and FSS frameworks. In Sec. V we discuss the case of Ising chains with symmetric boundaries, when we add symmetry-breaking boundary defects. In Sec. VI we present numerical analyses supporting the scaling behaviors obtained by the RG and FSS analyses. Finally, in Sec. VII we summarize and draw our conclusions.

II. QUANTUM ISING MODELS WITH SYMMETRY-BREAKING DEFECTS

The quantum Ising chain is a useful theoretical laboratory where fundamental issues of quantum many-body systems can be thoroughly investigated, exploiting the exact knowledge of several features of its phase diagram and quantum correlations. Many results for its low-energy properties have been derived in the ordered and disordered phases, and in particular at the quantum critical point separating the two phases, in the thermodynamic limit and in the FSS limit with various boundary conditions (see, e.g., Refs. [6,7,9,10] and references therein).

In our study of critical crossover behaviors driven by symmetry-breaking defects, we consider quantum Ising chains with ringlike geometry without boundaries and in the presence of one defect and chains with boundaries, such as OBC, in the presence of defects localized at the boundaries.

A. Quantum Ising rings with defects

Quantum Ising rings are defined by the Hamiltonian

$$\hat{H}_r = -J \sum_{x=1}^{L} \hat{\sigma}_x^{(1)} \hat{\sigma}_{x+1}^{(1)} - g \sum_{x=1}^{L} \hat{\sigma}_x^{(3)}, \qquad (1)$$

where L is the system size, $\hat{\sigma}_x^{(i)}$ are the Pauli matrices on the xth site ($i = 1, 2, 3$ labels the three spatial directions), and $\hat{\sigma}_{L+1}^{(i)} = \hat{\sigma}_1^{(i)}$, corresponding to PBC. In the following we assume ferromagnetic nearest-neighbor interactions with $J = 1$.

The model undergoes a CQT at $g = g_c = 1$, belonging to the two-dimensional Ising universality class, separating a disordered phase ($g > g_c$) from an ordered ($g < g_c$) one (see, e.g., Refs. [6,10]). Approaching the CQT, the system develops long-distance correlations, with length scales ξ diverging as $\xi \sim |g - g_c|^{-\nu}$ where $\nu = y_g^{-1} = 1$ and y_g is the RG dimension associated with the difference $g - g_c$. The ground-state energy gap gets suppressed as $\Delta \sim \xi^{-z}$ where z is the dynamic critical exponent $z = 1$. Another independent critical exponent arises from the RG dimension of the symmetry-breaking homogeneous longitudinal field h coupled to $\sum_x \hat{\sigma}_x^{(1)}$, which is $y_h = (2 + d + z - \eta)/2 = 2 - \eta/2$ where d stands for the system dimension (here $d = 1$) and $\eta = 1/4$, thus $y_h = 15/8$. We recall that, along the $|g| < 1$ line, the longitudinal field h drives quantum first-order transitions. Around g_c, the interplay between ξ and the size L of the system gives rise to FSS [10,29], defined as the large-L limit keeping ξ/L constant.

We want to study the effects of localized defects breaking the $\mathbb{Z}_2$ symmetry of model (1), such as the one described by the Hamiltonian term

$$\hat{D}_k = -\kappa \, \hat{\sigma}_k^{(1)}, \qquad (2)$$

where the parameter labeled by the Greek letter κ controls the strength of the defect, while the Roman index k denotes the defect site. Such a defect also breaks the translation invariance of the original model (1). Its effects within the first-order transition line for $g < g_c$ has been analyzed in Refs. [30,31], where it gives rise to a defect-driven CQT between different quantum phases. In the following, we focus on the critical crossover phenomena driven by $\hat{D}_k$ at the CQT for $g \approx g_c$.

We note that the defect (2) provides a bridge between translation-invariant systems with PBC for $\kappa = 0$ [cf. Eq. (1)] and models with PFBC when $\kappa \to \infty$ (due to the fact that the state at site k gets fixed to the eigenstate of $\hat{\sigma}_k^{(1)}$ with eigenvalue $s = 1$). Note that, in the presence of $n > 1$ equal defects like that in Eq. (2), the limit $\kappa \to \infty$ gives rise to an effective multipartition of the system, where the n subsystems separated by the defects can be considered as effectively disconnected chains with PFBC.

The effects of the local perturbation arising from defect may get amplified by long-distance correlations at CQTs. Although they do not alter the leading power-law behavior, scaling functions may acquire a nontrivial dependence on the external localized field, i.e., the parameter κ in Eq. (2). Indeed, as we shall see, one symmetry-breaking defect gives rise to a critical crossover behavior entailing substantial and rapid changes of the ground-state properties.

B. Quantum Ising chains with boundary defects

We also consider another class of symmetry-breaking defects, localized at the boundaries of the model. As we shall see, they give rise to similar critical crossover effects at quantum transitions, but characterized by different critical exponents. Quantum Ising chains with OBC are defined by the Hamiltonian

$$\hat{H}_b = -J \sum_{x=1}^{L-1} \hat{\sigma}_x^{(1)} \hat{\sigma}_{x+1}^{(1)} - g \sum_{x=1}^{L} \hat{\sigma}_x^{(3)}. \tag{3}$$

As before, we fix $J = 1$. We discuss the effects of longitudinal fields localized at the boundaries, such as those described by the Hamiltonian term

$$\hat{B} = -\zeta \left(\hat{\sigma}_1^{(1)} + \hat{\sigma}_L^{(1)} \right), \tag{4}$$

where ζ plays the role of parallel boundary field. This kind of defect allows us to interpolate between systems with OBC at $\zeta = 0$ and systems with PFBC in the limit $\zeta \to \infty$. The effects of boundary fields such as that in Eq. (4) have been already discussed in Ref. [32]. We will add further results to characterize the critical crossover that they give rise.

III. OBSERVABLES

A. Gap, magnetization, and two-point function

We define the gap Δ as the energy difference between the first excited state and the ground state. We recall that the power law of the asymptotic finite-size behavior of the gap is not changed by the presence of defects or by different choices of the boundary conditions. However, the amplitude of the leading behavior does depend on these features. For example, at the critical point one has

$$\Delta(L) = \frac{C_\Delta}{L} + O(L^{-2}), \tag{5}$$

with $C_\Delta = \pi/2$, π, 4π, respectively, for PBC, OBC, and PFBC [32–36].

We also address the expectation value of the longitudinal order-parameter operator $\hat{\sigma}_x^{(1)}$ on the ground state $|\Psi_0\rangle$, i.e., the magnetization,

$$M_x = \langle \Psi_0 | \hat{\sigma}_x^{(1)} | \Psi_0 \rangle, \tag{6}$$

its two-point correlation function

$$G(x, y) \equiv \langle \Psi_0 | \hat{\sigma}_x^{(1)} \hat{\sigma}_y^{(1)} | \Psi_0 \rangle, \tag{7}$$

as well as the corresponding susceptibility and correlation length,

$$\chi_x = \sum_y G(x, y), \quad \xi_x^2 = \frac{\sum_y D(x, y)^2 G(x, y)}{2\chi_x}, \tag{8}$$

where $D(x, y)$ is the minimum distance between the sites x and y (this definition takes into account the ring geometry). In our analyses of position-dependent observables, such as M_x, χ_x, and ξ_x, we consider particular values of x, such as the central site for chains with boundaries. For Ising rings with defect, one may choose either the site $x = k$ of the defect or the opposite site $x = k + L/2$ at the largest distance.

We also study the spatially averaged quantities

$$M_a = \frac{1}{L} \sum_x M_x, \quad \chi_a = \frac{1}{L} \sum_x \chi_x, \tag{9}$$

and

$$\xi_a^2 = \frac{\sum_{x,y} D(x, y)^2 G(x, y)}{2 \sum_x \chi_x}. \tag{10}$$

B. RG invariant quantities

To characterize the crossover behavior due to the defects, we consider a set of RG invariant quantities, which we will generically denote with R in the following. They are the ratios between the correlation lengths and the size:

$$R_{\xi x} \equiv \xi_x/L, \quad R_{\xi a} \equiv \xi_a/L. \tag{11}$$

Moreover we may consider ratios of correlation function at different scaling distance, such as

$$R_{Gx} \equiv \frac{G(x, x + X_1 L)}{G(x, x + X_2 L)}, \tag{12}$$

where X_1 and X_2 are fixed fractions of the size L, such as $X_1 = 1/2$ and $X_2 = 1/4$. A natural choice for Ising chains is that of identifying x with the center of the chain. For Ising rings one may also consider the average definition

$$R_{Ga} \equiv \frac{\sum_x G(x, x + X_1 L)}{\sum_x G(x, x + X_2 L)}. \tag{13}$$

We also consider the so-called Binder parameter depending on one point x,

$$U_x = \frac{\sum_{u,v,w} \langle \Psi_0 | \hat{\sigma}_x^{(1)} \hat{\sigma}_u^{(1)} \hat{\sigma}_v^{(1)} \hat{\sigma}_w^{(1)} | \Psi_0 \rangle}{L \left(\sum_u \langle \Psi_0 | \hat{\sigma}_x^{(1)} \hat{\sigma}_u^{(1)} | \Psi_0 \rangle \right)^2}, \tag{14}$$

or its spatially averaged version,

$$U_a = \frac{\sum_{x,u,v,w} \langle \Psi_0 | \hat{\sigma}_x^{(1)} \hat{\sigma}_u^{(1)} \hat{\sigma}_v^{(1)} \hat{\sigma}_w^{(1)} | \Psi_0 \rangle}{\left(\sum_{x,u} \langle \Psi_0 | \hat{\sigma}_x^{(1)} \hat{\sigma}_u^{(1)} | \Psi_0 \rangle \right)^2}. \tag{15}$$

C. Ground-state fidelity associated with the defect

To characterize the effects of the defects, we may also consider the ground-state fidelity quantifying the overlap between the ground states for different defect parameters (see, e.g., Refs. [10,37–39]). The usefulness of the fidelity as a tool to distinguish quantum states can be traced back to Anderson's orthogonality catastrophe [40]: the overlap of two many-body ground states corresponding to Hamiltonians differing by a small perturbation vanishes in the thermodynamic limit. Besides that, the corresponding fidelity susceptibility covers a central role in quantum estimation theory [41,42], being proportional to the so-called quantum Fisher information. The latter indeed quantifies the inverse of the smallest variance in the estimation of the varying parameter, such that, in proximity of quantum transitions, metrological performances are believed to drastically improve [43,44].

To monitor the changes of the ground-state wave function $|\Psi_0(L, g, \kappa)\rangle$ when varying the defect strength κ by a small amount $\delta\kappa$ (keeping the Hamiltonian parameter g fixed), we

define the fidelity

$$A(L, g, \kappa, \kappa + \delta\kappa) \equiv |\langle\Psi_0(L, g, \kappa + \delta\kappa)|\Psi_0(L, g, \kappa)\rangle| . \tag{16}$$

Assuming $\delta\kappa$ sufficiently small, one can expand Eq. (16) in powers of $\delta\kappa$:

$$A(L, g, \kappa, \delta\kappa) = 1 - \tfrac{1}{2}\delta\kappa^2 A_2(L, g, \kappa) + O(\delta\kappa^3), \tag{17}$$

where

$$A_2(L, g, \kappa) = \left.\frac{\partial^2 A}{\partial \delta\kappa^2}\right|_{\delta\kappa=0}, \tag{18}$$

represents the fidelity susceptibility [10,38]. The cancellation of the linear term in the expansion (17) is essentially related to the fact that the fidelity is bounded [38], i.e., $1 \geqslant A \geqslant 0$. One may also consider analogous definitions for the model (3) with the boundary fields (4), by replacing κ with ζ in the above equations.

IV. CRITICAL CROSSOVER DRIVEN BY SYMMETRY-BREAKING DEFECTS

We start to consider the case of the Ising ring with one symmetry-breaking defect [cf., Eq. (2)], whose location is irrelevant, since the original model (1) is invariant under translations.

A. Critical crossover behavior driven by the defect

We first show that the perturbation arising from the defect is relevant in critical Ising rings, i.e., the RG dimension y_κ of the corresponding parameter κ is positive. One can straightforwardly determine y_κ by analyzing the corresponding perturbation to the translationally invariant field theory. This can be written as

$$P_\kappa = \kappa \int d\tau \, \varphi(x, \tau), \tag{19}$$

where $\varphi(x, \tau)$ is the order-parameter field of the Ising transition, and the integration is over the Euclidean time τ. There is no integration over the space, because the perturbation is spatially localized (note that the location of the defect is assumed to be within the bulk, i.e., it is not close to a boundary). The standard RG analysis of the perturbation P_κ entails a relation among the RG dimensions of the quantities entering its definition, given by

$$y_\kappa + y_\varphi - z = 0, \tag{20}$$

where

$$y_\varphi = (d + z - 2 + \eta)/2 = 1/8 \tag{21}$$

is the RG dimension of the order-parameter field [6,10]. Thus we obtain

$$y_\kappa = z - y_\varphi = 7/8 . \tag{22}$$

We are now in the position to put forward the scaling behaviors of the various observables introduced in Sec. III, within a standard FSS framework [10–13,15–17,33]. Since the RG dimension of the defect parameter κ is positive, the defect gives rise to a relevant perturbation, whose effect is that of moving away from the FSS behavior of the Ising ring

(1), characterized by translation invariance and intact $\mathbb{Z}_2$ symmetry. The corresponding FSS limit of generic observables is defined as the large-size limit keeping the scaling variables

$$W = (g - g_c)L^{y_g}, \quad K = \kappa L^{y_\kappa}, \tag{23}$$

fixed (we recall that $y_g = \nu^{-1} = 1$ for one-dimensional quantum Ising models). This defines the critical crossover regime driven by the defect, which develops around $\kappa = 0$, for $|\kappa| \sim L^{-y_\kappa}$.

B. Critical crossover behavior of the observables

The critical crossover behaviors of the various quantities introduced in Sec. III can be put forward as follows. The gap is expected to behave as

$$\Delta(L, g, \kappa) \approx L^{-z}\mathcal{D}(W, K), \tag{24}$$

where $\mathcal{D}(W, K)$ is a universal scaling function, i.e., microscopic variations of the Ising ring Hamiltonian, for example, adding further next-to-nearest-neighbor couplings between the spin operators, do not change it (apart from trivial normalizations of the arguments).

The magnetization in the FSS limit is expected to behave as

$$M_x(x, L, g, \kappa) \approx L^{-y_\varphi}\mathcal{M}_x(X_k, W, K), \tag{25a}$$

$$M_a(L, g, \kappa) \approx L^{-y_\varphi}\mathcal{M}_a(W, K), \tag{25b}$$

where y_φ is the RG dimension of the order-parameter field [cf. Eq. (21)] and

$$X_k = x_k/L, \quad x_k = \text{Min}[x - k, L - x + k], \tag{26}$$

where x_k is the distance from the defect along the ring. Analogously, for two-point correlation functions we find

$$G(x, y, L, g, \kappa) \approx L^{-2y_\varphi}\mathcal{G}(X_k, Y_k, W, K), \tag{27}$$

where $Y_k = y_k/L$, and y_k is defined analogously to x_k. Using the above results, we may easily derive the FSS behaviors of the RG invariant quantities R defined in Eqs. (11), (12), and (13), obtaining

$$R_x(x, L, g, \kappa) \approx \mathcal{R}_x(X_k, W, K), \tag{28a}$$

$$R_a(L, g, \kappa) \approx \mathcal{R}_a(W, K) . \tag{28b}$$

Analogous scaling behaviors are expected for the Binder parameters U_x and U_a; cf. Eqs. (14) and (15).

We remark that the above FSS behaviors are defined in the large-L limit keeping all arguments of the scaling functions fixed, and in particular $K = \kappa L^{y_\kappa}$. They reflect the fact that the perturbation arising from the symmetry-breaking defect is relevant, thus affecting, and changing, the asymptotic translation-invariant FSS functions of the original Ising ring. We stress again that, unlike quantum first-order transitions [45,46], they cannot change the bulk power laws at CQTs, but only the FSS functions [10].

As already mentioned above, the $\kappa \to \infty$ limit of the defect strength gives rise to systems with PFBC. Therefore we may interpret the above-reported FSS behaviors as a critical crossover from the FSS of the translation-invariant Ising ring to that of systems with PFBC, which is asymptotically realized for any finite value of $\kappa > 0$. Therefore, we expect that

the limit $K \to \infty$ of the scaling functions converges to the FSS functions for PFBC, which are realized for any finite $\kappa > 0$ asymptotically in the large-L limit.

In particular, the critical gap should behave as

$$\Delta(L, g, \kappa > 0) \approx L^{-z}\mathcal{D}_{\text{pfbc}}(W), \quad (29)$$

for any finite $\kappa > 0$, where $\mathcal{D}_{\text{pfbc}}(W)$ is the scaling function associated with the gap of Ising chains with PFBC,

$$\Delta_{\text{pfbc}}(L, g) \approx L^{-z}\mathcal{D}_{\text{pfbc}}(W), \quad \mathcal{D}_{\text{pfbc}}(0) = 4\pi, \quad (30)$$

and we also used Eq. (5). Moreover, we expect that

$$\mathcal{D}(W, K \to \infty) = \mathcal{D}_{\text{pfbc}}(W). \quad (31)$$

Analogous considerations apply to the other observables. For example, in the case of the RG invariant quantities R_a, whose scaling is reported in Eq. (28b),

$$R_a(L, g, \kappa > 0) \approx \mathcal{R}_{\text{pfbc}}(W) = \mathcal{R}(W, K \to \infty), \quad (32)$$

when taking the FSS limit, keeping $\kappa > 0$ fixed.

We finally remark that the critical crossover behaviors driven by symmetry-breaking defects may appear analogous to those arising from relevant perturbations at a unstable fixed point of the homogeneous theory, driving away the RG flow toward another stable fixed point.

C. Scaling corrections

The asymptotic FSS behaviors are generally approached with power-law suppressed corrections [10,33], which may depend on the observable considered. Within CQTs belonging to the two-dimensional Ising universality class, the contributions of the leading irrelevant operator are suppressed as $L^{-\omega}$ with $\omega = 2$ [33,47,48]. Moreover the leading corrections related to the breaking of the rotational invariance on the lattice are suppressed as $L^{-\omega_{\text{nr}}}$ with $\omega_{\text{nr}} = 2$, as well [47,49,50]. However, there are also corrections that are suppressed more slowly. Some quantities are subject to corrections from analytic background contributions [33], for example, those involving second-moment correlation lengths [cf. Eq. (11)], for which the leading scaling corrections get suppressed as $L^{-(1-\eta)} = L^{-3/4}$ only, even in the case of systems without boundaries.

The existence of the defect, breaking translation invariance, gives generally rise to $O(1/L)$ corrections. However, when studying the effects of its perturbation in the $\kappa \to 0$ limit keeping κL^{y_κ} fixed, the leading scaling corrections are those arising from the analytic expansion [33] of the scaling field u_κ associated with the defect parameter κ. In particular at the critical point $g = g_c$, taking into account the parity property of the defect term, we expect

$$u_\kappa \approx \kappa + c\,\kappa^3 + \cdots . \quad (33)$$

Since the FSS limit is actually obtained by keeping the product $u_\kappa L^{y_\kappa}$ fixed, involving the analytic scaling field [10,33], the third-order correction in Eq. (33) gives rise to $O(L^{-2y_\kappa})$ scaling corrections, with $2y_\kappa = 7/4$, which decay more slowly than those arising from the leading irrelevant operators of the two-dimensional Ising universality class.

D. Critical crossover of the defect fidelity

A discussion of the FSS behavior of the ground-state fidelity associated with homogeneous variations of the system Hamiltonian, within the critical region (around $g = g_c$), can be found in Refs. [10,51]. Extending these scaling arguments to the case of localized variations, we arrive at a scaling hypothesis for the critical nonanalytic part at the CQT and around $\kappa = 0$:

$$A(L, g, \kappa, \delta\kappa)_{\text{sing}} \approx \mathcal{A}(W, K, \delta K), \quad \delta K \equiv \delta\kappa\, L^{y_\kappa}. \quad (34)$$

The behavior of its susceptibility A_2 is then obtained from Eq. (34), by expanding $\mathcal{A}$ in powers of δK, and matching it with Eq. (17):

$$A_2(L, g, \kappa)_{\text{sing}} \approx \left(\frac{\delta K}{\delta\kappa}\right)^2 \mathcal{A}_2(W, K) = L^{2y_\kappa}\mathcal{A}_2(W, K). \quad (35)$$

The above asymptotic FSS behaviors are expected to be approached with $O(L^{-2y_\kappa})$ corrections; see Sec. IV C.

Note that for finite values of $\kappa > 0$, i.e., keeping $\kappa > 0$ fixed in the large-size limit, the above FSS behavior is not expected to hold anymore. Indeed, since the asymptotic FSS behavior does not change for any $\kappa > 0$, we simply expect that the variation of the fidelity is much smoother, due to the fact that the ground states for $\kappa > 0$ and $\kappa + \delta\kappa$ are expected to differ only in a finite region around the defect. Therefore, its susceptibility is not expected to diverge with increasing the lattice size:

$$A_2(L, g, \kappa > 0) = O(1). \quad (36)$$

The above behaviors of the fidelity and its susceptibility will be confirmed by numerical computations.

V. CRITICAL CROSSOVER DRIVEN BY BOUNDARY DEFECTS

We now discuss the case of Ising systems with boundaries, such as that defined in Eq. (3) with OBC, in the presence of parallel boundary fields as those in Eq. (4), which also give rise to a relevant perturbation. Changing ζ from 0 to ∞ moves the system from the symmetric OBC to the PFBC that violate the global $\mathbb{Z}_2$ symmetry. The main difference with the case of defects within rings is that the RG dimension of boundary fields φ_b differs from that of fields in the bulk. Indeed, within the two-dimensional universality class, its scaling dimension turns out to be $y_b = 1/2$ [14–16], instead of the bulk value $y_\varphi = 1/8$. Thus, using the same formula (22), after replacing y_φ with y_b, we obtain

$$y_\zeta = z - y_b = 1/2. \quad (37)$$

The corresponding scaling variable is given by

$$Z = \zeta\, L^{y_\zeta}. \quad (38)$$

The critical crossover driven by the boundary fields is expected to hold in the large-L limit keeping Z fixed, thus for $\zeta \sim L^{-y_\zeta}$.

The critical crossover of the gap is described by the scaling equation [32]

$$\Delta(L, g, \zeta) \approx L^{-z}\mathcal{D}(W, Z). \quad (39)$$

On the other hand, its finite-ζ behavior scales as

$$\Delta(L, g, \zeta > 0) \approx L^{-z} \mathcal{D}_{\text{pfbc}}(W) \tag{40}$$

independently of $\zeta > 0$, where $\mathcal{D}_{\text{pfbc}}(W)$ is the FSS function of the gap with PFBC. We again expect that

$$\mathcal{D}(W, Z \to \infty) = \mathcal{D}_{\text{pfbc}}(W). \tag{41}$$

Therefore, systems with boundary defects of finite strength $\zeta > 0$ develop the same FSS of those with PFBC, independently of the actual value of ζ.

The scaling behavior of Eqs. (39) and (40) has been analytically shown to hold in Ref. [32]. In particular, at the critical point $g = g_c$, the critical crossover interpolates between the value $\mathcal{D}(W, Z = 0) = \pi$ [corresponding to the amplitude of the gap for systems with OBC; cf. Eq. (5)] to $\mathcal{D}(W, Z = \infty) = 4\pi$ (corresponding to the amplitude of the gap for systems with PFBC).

The magnetization and correlation functions are expected to behave as

$$M_x(x, L, g, \zeta) \approx L^{-y_\varphi} \mathcal{M}_x(X, W, Z), \tag{42}$$

$$G(x, y, L, g, \zeta) \approx L^{-2y_\varphi} \mathcal{G}(X, Y, W, Z), \tag{43}$$

where $X = x/L$ and $Y = y/L$. Analogous FSS equations are obtained for the other quantities defined in Sec. III. For example, we may consider the most natural definition of second-moment correlation (8), taking $\xi \equiv \xi_x$ with x located at the center of the chain, and obtain

$$R_\xi(L, g, \zeta) \equiv \xi/L \approx \mathcal{R}_\xi(W, Z). \tag{44}$$

We can also derive scaling formulas for the ground-state fidelity associated with the boundary fields, analogous to those for the Ising ring with one defect, by replacing K with Z, and δK with δZ:

$$A(L, g, \zeta, \delta\zeta)_{\text{sing}} \approx \mathcal{A}(W, Z, \delta Z), \quad \delta Z \equiv \delta\zeta\, L^{y_\zeta}, \tag{45}$$

$$A_2(L, g, \zeta) \approx L^{2y_\zeta} \mathcal{A}_2(W, Z). \tag{46}$$

Note that even boundary defects give rise to a power-law growth of A_2 when increasing L, but this is significantly slower than the case of bulk defects; indeed, $A_2 \sim L$ since $y_\zeta = 1/2$. Again for finite fixed ζ we expect $A_2(L, g, \zeta) = O(1)$.

The power-law approach to the above asymptotic FSS behaviors can be inferred by the analysis reported in Sec. IV C. The leading scaling corrections are generally expected to be $O(L^{-1})$, arising from the presence of the boundaries and the analytic expansion of the scaling field associated with ζ (since $2y_\zeta = 1$). A slower approach should still characterize the observables involving second-moment correlation length, as $L^{-3/4}$, due to background contributions.

We finally note that Ising chains with OBC and in the presence of symmetry-breaking defects in the bulk (i.e., far from the boundaries), such as those described by the Hamiltonian term (2), are expected to develop a critical crossover behavior driven by the defect as well, similar to that of quantum Ising rings, discussed in Sec. IV. While the scaling behavior is still controlled by the RG dimension $y_\kappa = 7/8$, the corresponding
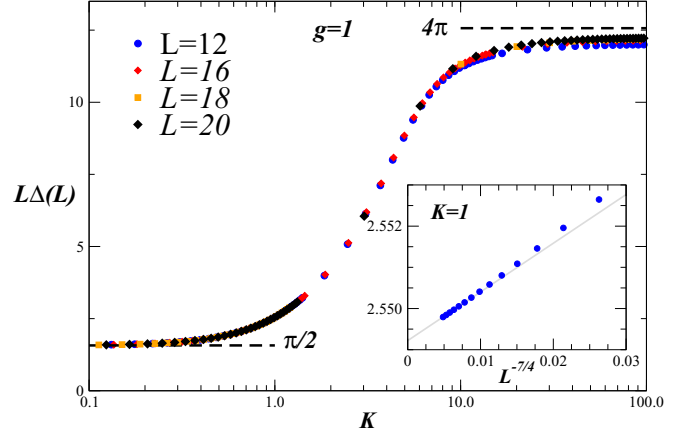

FIG. 1. Critical crossover of the gap $\Delta(L, g, \kappa)$ at the critical point $g_c = 1$. The collapse of the data of $L^z \Delta$ vs $K = \kappa L^{y_\kappa}$ (with $z = 1$ and $y_\kappa = 7/8$) supports the scaling behavior reported in Eq. (24). The dashed lines indicate the limiting cases: $\mathcal{D}(0, K \to 0) = \pi/2$ and $\mathcal{D}(0, K \to \infty) = 4\pi$, which can be obtained from Eq. (5), corresponding to PBC and PFBC. The inset shows that the scaling corrections at $K = 1$ are consistent with the expected $O(L^{-7/4})$ suppression; see Sec. IV C (the gray line is drawn to guide the eye).

scaling functions are expected to differ, because they interpolate between a system with OBC (when $\kappa = 0$) and the $\kappa \to \infty$ limit consisting of a system with two subsystems of size L_1 and L_2 (where L_1, L_2 are the distances of the defect from the boundaries) having mixed boundary conditions: OBC on one side and fixed boundary conditions on the other one (corresponding to the position of the defect).

VI. NUMERICAL RESULTS

To support the scaling behaviors put forward in the previous sections, we now present some numerical results, obtained by exact diagonalization (up to $L = 20$ sites) and by density-matrix renormalization group (DMRG) for larger systems (up to $L = 40$; see the Appendix for details of the implementation for systems with PBC). Note that, unlike Ising chains in the presence of symmetry-preserving bond defects, we cannot exploit the Jordan-Wigner transformation to map the system into a quadratic fermionic model, due to the presence of $\mathbb{Z}_2$ symmetry-breaking longitudinal fields. Indeed, the nonlocality of the Jordan-Wigner transformation cannot be reabsorbed in the presence of the symmetry-breaking defect given in Eq. (2), giving rise to nontrivial string terms of fermionic operators.

A. Critical defect crossover in Ising rings

We first report results supporting the critical crossover behavior driven by the symmetry-breaking defect (2) in quantum Ising rings, as discussed in Sec. IV. These are obtained around the critical point $g_c = 1$; actually most of them are exactly at $g = g_c$.

The energy difference between the two lowest levels (i.e., the gap) at the critical point is reported in Fig. 1. The behavior of the various curves for different sizes L matches the scaling
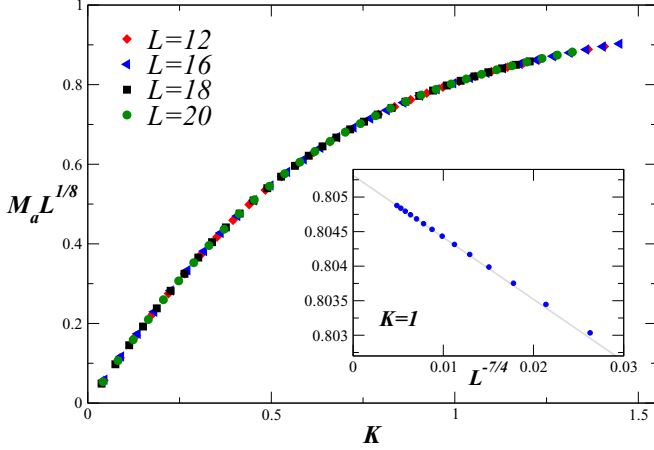
FIG. 2. Critical crossover of the average magnetization M_a, defined in Eq. (6), at the critical point $g_c = 1$. The figure shows the rescaled data $L^{y_\varphi} M_a$ vs $K = \kappa L^{y_\kappa}$, with $y_\varphi = 1/8$ and $y_\kappa = 7/8$. The collapse of the data for various lattice sizes along a universal FSS curve supports the scaling in Eq. (25b). The inset shows that the scaling corrections at a fixed value $K = 1$ are consistent with the expected $O(L^{-7/4})$ behavior; see Sec. IV C (the gray line is drawn to guide the eye).

FIG. 3. The correlation length ξ_a, defined in Eq. (10), along the critical defect crossover at the critical point $g_c = 1$. We plot the ratio $\xi_a/\xi_{a,0}$ vs $K = \kappa L^{y_\kappa}$, where $\xi_{a,0}$ is the correlation length at $\kappa = 0$; see also Eq. (47). The data approach an asymptotic scaling function, in agreement with the scaling equation (28b). The inset shows that the scaling corrections at a fixed value $K = 1$ are consistent with the asymptotic power-law $O(L^{-3/4})$ suppression; see Sec. IV C. (the gray line is drawn to guide the eye).

ansatz (24). In particular, data for $L\,\Delta(L)$ as a function of $K = \kappa L^{y_\kappa}$ range from $\pi/2$ to 4π, consistent with the crossover from PBC to PFBC. In fact, the amplitude C_Δ of the leading behavior $\Delta \approx C_\Delta/L$ at the critical point goes from $C_\Delta = \pi/2$, for systems without boundaries corresponding to $\kappa = 0$, to $C_\Delta = 4\pi$, in the $K \to \infty$ limit of PFBC corresponding to finite κ.

In Fig. 2 we report some results for the averaged magnetization defined in Eq. (6) at $g = g_c$. While the bare data points behave differently for various system sizes, a nice data collapse when plotting $L^{1/8} M_a$ vs $K = \kappa L^{7/8}$ is observed, thus supporting the FSS ansatz (25b). Leading scaling corrections are $O(L^{-7/4})$, coming from the analytical expansion (33) of the defect scaling field.

Further evidence of the critical crossover is provided by a numerical analysis of the ratio

$$\frac{\xi_a}{\xi_{a,0}} \equiv \frac{\xi_a(L, g = g_c, \kappa)}{\xi_a(L, g = g_c, \kappa = 0)} = \frac{R_\xi(L, g = g_c, \kappa)}{R_\xi(L, g = g_c, \kappa = 0)}, \quad (47)$$

presented in Fig. 3. Note that the analysis of the ratio $\xi_a/\xi_{a,0}$, instead of ξ_a/L, turns out to be cleaner, because it is subject to smaller scaling corrections, somehow suppressing those that are already present at the critical point for $\kappa = 0$. The data appear to approach an asymptotic scaling function, in agreement with the scaling equation (28b). In this case, the leading scaling corrections to R_ξ are $O(L^{-3/4})$ (see also the inset of Fig. 3) coming from the analytical background at the CQT (see the discussion in Sec. IV C).

The above results definitely confirm the scaling predictions for the critical crossover behavior driven by the defects, moving away from the translation-invariant and $\mathbb{Z}_2$-symmetric FSS of the critical Ising ring (1).
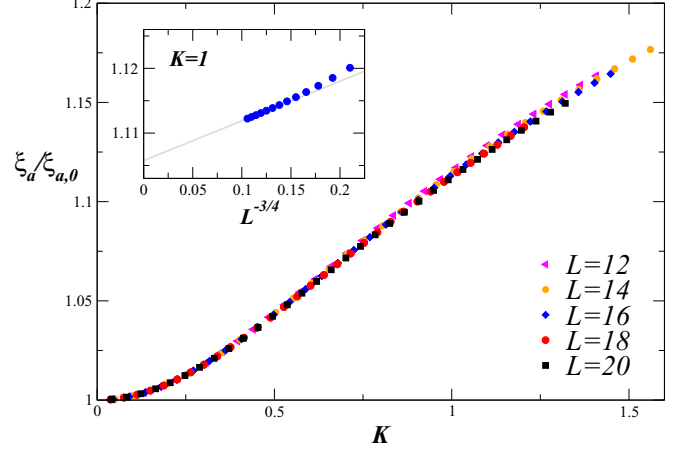
1. The defect ground-state fidelity

Interesting features of the critical crossover driven by defects emerge when looking at the ground-state fidelity [cf. Eq. (16)]. As discussed in Sec. IV D, we expect that the fidelity, and in particular the associated susceptibility (18), exhibits qualitatively different behaviors around $\kappa = 0$ and for any finite and fixed $\kappa > 0$.

In Fig. 4 we report some results for the fidelity A at the critical point and for $\kappa = 0$, as a function of $\delta\kappa$. The top panel shows the fidelity as a function of $\delta\kappa$, which appear suppressed at smaller and smaller values of $\delta\kappa$, when increasing the system size. Plotting the same data vs $\delta K = \delta\kappa L^{y_\kappa}$, with $y_\kappa = 7/8$, a nice collapse toward an asymptotic curve emerges, thus supporting the FSS behavior (34) (bottom panel). Corrections to the asymptotic FSS are suppressed consistently with the power law $L^{-7/4}$, as expected from the analysis of Sec. IV C.

Figure 5 shows results for the fidelity susceptibility A_2 at the critical point $g = g_c$ [52]. They confirm the scaling Eq. (35), and in particular that in the critical crossover regime A_2 diverges as $L^{2y_\kappa} = L^{7/4}$ with increasing L. This shows that, at the critical point and around $\kappa = 0$, the impact of the defect (2) on the system ground state is quite strong.

Finally we have also done the analogous computations for $\kappa = 1$, therefore relatively far from the critical crossover region where $\kappa \sim L^{-y_\kappa}$ is involved in the critical defect crossover around $\kappa = 0$. As shown in Fig. 6, the ground-state fidelity for $\kappa = 1$ and $\delta\kappa > 0$ becomes rapidly independent of L with increasing system size. This implies that the corresponding fidelity susceptibility A_2 remains finite with increasing L, as predicted by Eq. (36). This behavior turns out very different from the anomalous L^{2y_k} divergence characterizing the critical crossover behavior around $\kappa = 0$.
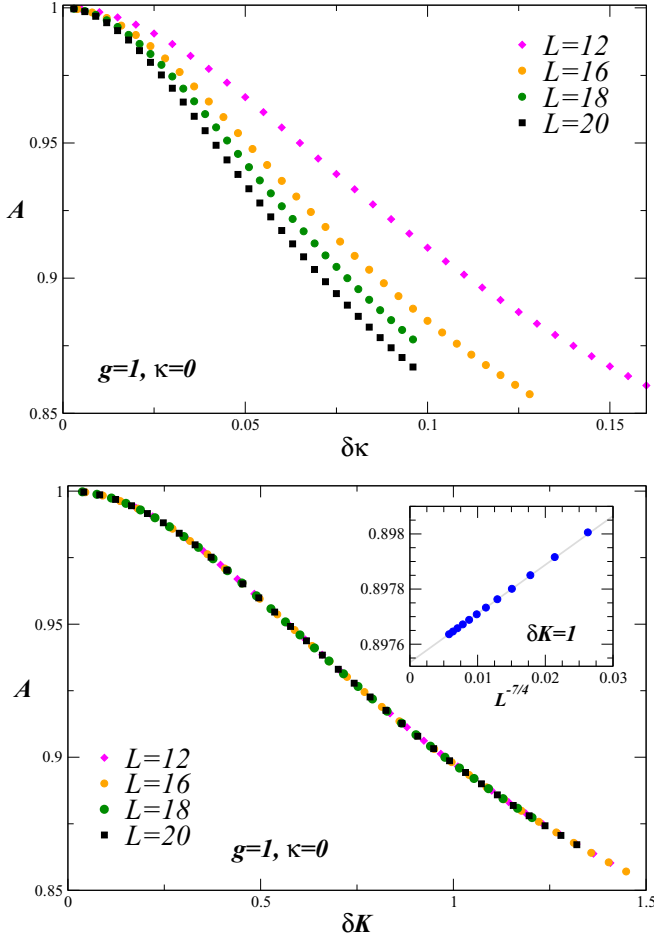
FIG. 4. The ground-state fidelity (16) associated with the defect, at the critical point $g_c = 1$. The top panel reports the plain data for $\kappa = 0$ as a function of $\delta\kappa$, showing that they tend to get suppressed at smaller and smaller values of $\delta\kappa$ when increasing the size of the system. The bottom panel shows them vs $\delta K = \delta\kappa L^{y_\kappa}$. The clear collapse of the curves definitely supports the scaling behavior (34). The inset of the bottom figure shows that the scaling corrections at $\delta K = 1$ are consistent with the expected $O(L^{-7/4})$ decay; see Sec. IV C.

B. Critical crossover arising from boundary defects

We now consider boundary defects such as those arising from boundary fields in Ising chains; cf. Eq. (4). Some results for the critical crossover of the gap have been already reported in Ref. [32]. Here we supplement them with results for the ground-state fidelity measuring the overlap of the ground states for different values of the boundary-field parameter ζ.

As discussed in Sec. V, we expect a critical crossover scenario analogous to that found for Ising rings, with the main difference that the fidelity susceptibility is expected to diverge as L^{2y_ζ}, thus as L, with increasing the size, at criticality and around $\zeta = 0$. The results in Fig. 7 nicely confirm these predictions. We also explicitly checked that corrections to the asymptotic FSS are suppressed as L^{-1}, as expected from the analysis of Sec. IV C (data not shown). On the other hand, like for bulk defects, the fidelity susceptibility for finite $\zeta > 0$ converges to a constant. This is demonstrated by the data for
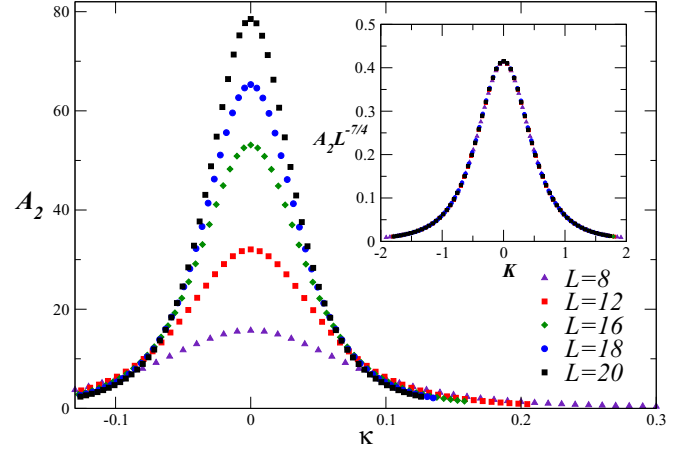

FIG. 5. The fidelity susceptibility A_2 [cf. Eq. (17)] associated with one defect within Ising rings, at the critical point $g_c = 1$ and around $\kappa = 0$. Note that, by symmetry, A_2 is invariant under $\kappa \rightarrow -\kappa$. The plain data already suggest that A_2 around $\kappa = 0$ diverges with increasing L. The inset shows a plot of $L^{-2y_\kappa} A_2$ vs $K = \kappa L^{y_\kappa}$ with $y_\kappa = 7/8$, which represents robust evidence in favor of the scaling behavior (35) and in particular the $L^{7/4}$ divergence with increasing L.

the fidelity at $\zeta = 1$ as a function of $\delta\zeta$, shown in Fig. 8, which appear to rapidly converge to a function of $\delta\zeta$ independent of L.

C. FSS keeping the defect strength fixed

Let us go back to the quantum Ising ring (1) with one symmetry-breaking defect (2). As a final check of the critical crossover scenario, we provide numerical evidence that the asymptotic FSS for $\kappa > 0$ does not depend on κ, and it corresponds to that for $\kappa \rightarrow \infty$, when the system becomes
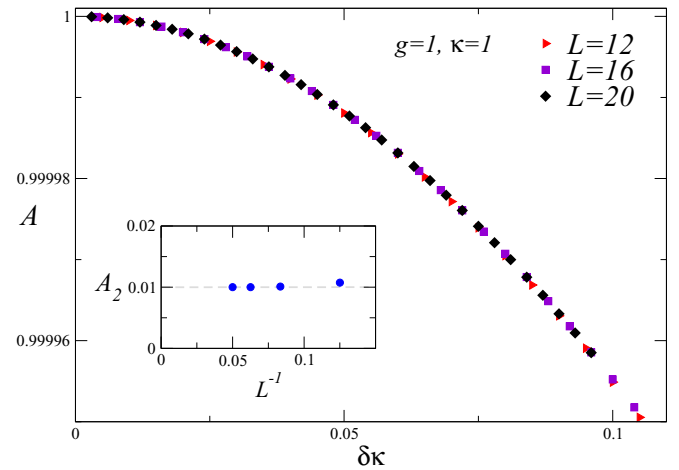

FIG. 6. The ground-state fidelity at the critical point, for $\kappa = 1$ vs $\delta\kappa$. With increasing system size, the curves become rapidly independent of L, thus implying that the corresponding fidelity susceptibility A_2 remains finite with increasing L. This is clearly visible from the data for A_2 shown in the inset, which appear to clearly approach a constant value with increasing L.
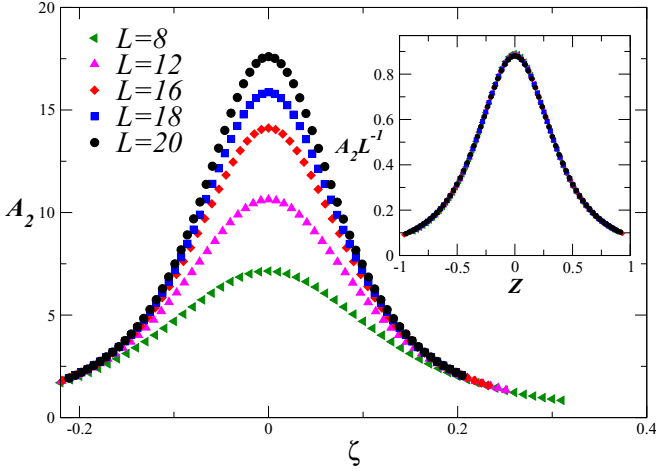
FIG. 7. The fidelity susceptibility A_2, associated with the boundary defects within Ising chains with OBC, at the critical point $g_c = 1$ and around $\zeta = 0$. Note that, by symmetry, A_2 is invariant under $\zeta \rightarrow -\zeta$. The inset shows a plot of $L^{-2y_\zeta} A_2$ vs $Z = \zeta L^{y_\zeta}$ with $y_\zeta = 1/2$. The data clearly support the RG prediction that A_2 diverges as L^{2y_ζ}, within the critical crossover region, keeping Z fixed.

equivalent to an Ising chain with PFBC. In other words, the FSS limit keeping $\kappa > 0$ fixed must be independent of κ, as discussed at the end of Sec. IV B; see in particular Eq. (32).

To avoid problems arising from possible change of normalizations of the scaling variable W, we proceed as follows. We consider the RG invariant quantities introduced in Sec. III. In particular, we consider $R_\xi \equiv R_{\xi x}$, $R_G \equiv R_{Gx}$, and $U \equiv U_x$; cf. Eqs. (11), (12), and (14), with x given by the position of the defect. Their FSS behavior for $\kappa > 0$ must generally be $R(L, g) \approx \mathcal{R}(W)$ independently of κ. Since R_ξ is a monotonic function, for $\kappa > 0$, we may also write

$$U(L, g, \kappa) \approx F_U(R_\xi), \quad R_G(L, g, \kappa) \approx F_G(R_\xi), \quad (48)$$
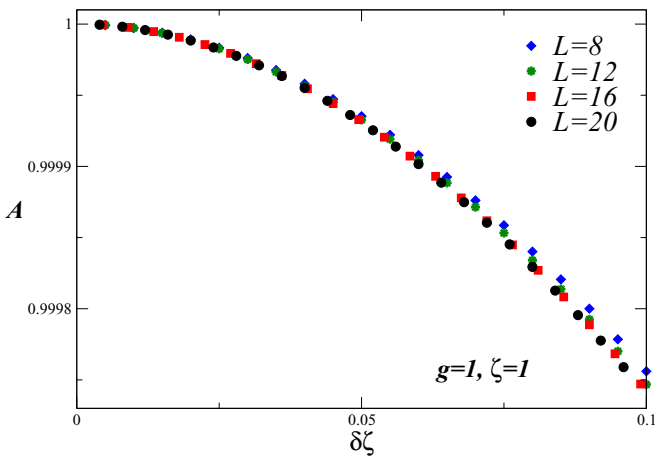

FIG. 8. The ground-state fidelity at the critical point, for $\zeta = 1$ vs $\delta\zeta$. With increasing the system size, the curves become rapidly independent of L, implying that the corresponding fidelity susceptibility A_2 remains finite with increasing L. This behavior is very different from the L^{2y_ζ} divergence characterizing the critical crossover behavior around $\zeta = 0$; see Fig. 7.
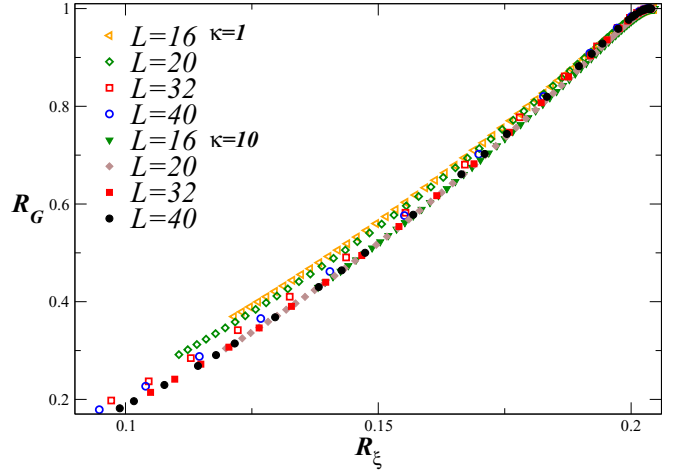

FIG. 9. Plots of R_G vs R_ξ for $\kappa = 1, 10$. Data for $\kappa = 1$ and $\kappa = 10$ appear to approach the same asymptotic curve. Data for $L = 32, 40$ are obtained by means of DMRG.

where F_U and F_G depend on the universality class only, without free normalizations. Numerical results in Fig. 9, for $\kappa = 1$ and $\kappa = 10$, confirm that R_G approaches the same scaling function of R_ξ, independently of κ. Analogous evidence has been found for U (not shown).

As a further check, in Fig. 10 we show data for the averaged quantity $R_{\xi a}$ defined in Eq. (11) evaluated at $g = g_c$, for $\kappa = 1$ and $\kappa = 10$. They show that the large-L extrapolations using the expected $L^{-3/4}$ asymptotic behavior are compatible between $\kappa = 1$ and $\kappa = 10$, and are definitely different from the value at $\kappa = 0$. Therefore, concerning the behavior at finite $\kappa > 0$, outside the critical crossover regime where $\kappa \sim L^{-y_\kappa}$, the numerical results confirm that the asymptotic FSS behavior is independent of the defect strength $\kappa > 0$, whenever they are computed keeping κ fixed.

Finally, we note that the average quantities R_{Ga} and U_a [defined in Eqs. (13) and (15)] when plotted vs $R_{\xi a}$ [defined in Eq. (11)] show universal curves that look very similar when
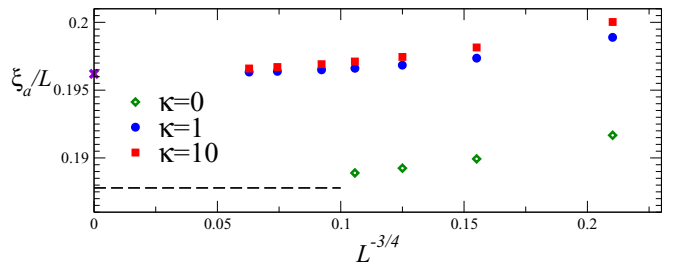

FIG. 10. Data for $R_{\xi a}$ vs $L^{-3/4}$ at the critical point and for $\kappa = 1, 10$, compared with the value for $\kappa = 0$ given by the exact result $R_{\xi a}^\star = 0.187789\ldots$ (indicated by the dashed line), easily obtained from the critical two-point function [7]. We also show some data at $\kappa = 0$ for relatively small lattice sizes, to highlight how the $\kappa = 0$ data approach the asymptotic exact value with increasing L. The large-L extrapolations for $\kappa = 1, 10$ are compatible with each other, and approximately equal to $R_{\xi a}^\star \approx 0.1962$ (violet cross in the plot), differing from the value at $\kappa = 0$. They support the fact that the FSS at finite fixed $\kappa > 0$ is expected to be independent of κ.
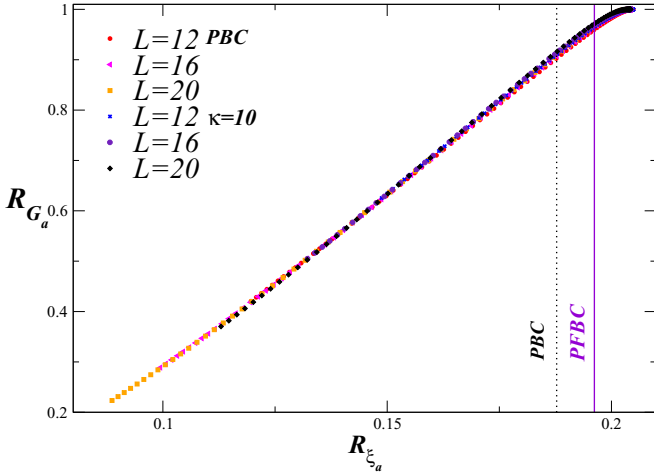
FIG. 11. The averaged quantities R_{Ga} vs $R_{\xi a} \equiv \xi_a/L$. The vertical dotted black and straight violet lines represent, respectively, the $R_{\xi a}^\star$ critical values for PBC and PFBC, corresponding to the limiting cases of critical defect crossover for $\kappa = 0$ and $\kappa \to \infty$. Although their values at $g = g_c$, indicated by the vertical lines, differ significantly (see also Fig. 10), the FSS curves of the averaged quantities turn out to be very similar when moving from $\kappa = 0$ to a finite κ.

moving from $\kappa = 0$ to a finite κ, i.e., from PBC to PFBC. This is shown, e.g., in Fig. 11, where we plot R_{Ga} vs $R_{\xi a}$ for $\kappa = 0$ and $\kappa = 10$. Actually, this is quite unexpected: although the values of R_{Ga} and $R_{\xi a}$ at $g = g_c$ differ significantly ($R_{\xi a} \approx 0.1878$ for $\kappa = 0$ and $R_{\xi a} \approx 0.1962$ for $\kappa = 10$), the FSS curves of the averaged quantities for $\kappa = 0$ and $\kappa > 0$ turn out to be very close.

VII. CONCLUSIONS

We have investigated the effects of symmetry-breaking defects at CQTs, arising from localized external fields coupled to the order-parameter operator. At CQTs the presence of isolated defects does not generally change the bulk power-law behaviors of observables at large scale. However, when the defects are the only source of symmetry breaking (i.e., the original lattice system is strictly symmetric under the global symmetry, without boundaries or with boundaries preserving the symmetry), they drive critical crossover behaviors entailing substantial and rapid changes of the ground-state and low-energy properties. The limiting cases of these critical defect crossovers can be associated with different boundary conditions: from boundary conditions preserving the global symmetry to ones breaking the symmetry. Therefore, the addition of symmetry-breaking defects can drive relevant effects in finite-size systems (or in the neighborhood of the defect), leading to substantial changes in the finite-size behavior of the low-energy critical modes, even in the large-size limit within the FSS regime around the CQT. Two different situations must be distinguished: whether the defects are located within the bulk of the system or at the boundaries. Indeed, they lead to scaling scenarios controlled by different RG exponents associated with the universality class of the CQT.

The above scenario has been investigated within the paradigmatic one-dimensional quantum Ising models in a transverse field, whose CQT is related to the spontaneous breaking of a global $\mathbb{Z}_2$ symmetry. We analyze the effects of localized defects breaking the global $\mathbb{Z}_2$ symmetry, arising from external longitudinal fields localized at one site of the system. We consider both bulk and boundary defects.

Using standard RG arguments within FSS frameworks, we develop a scaling theory to describe the critical crossover behaviors driven by the symmetry-breaking defects. In particular, one localized symmetry-breaking defect in critical Ising rings turns out to develop a critical crossover between translation-invariant Ising rings without boundaries and Ising systems with fixed and parallel boundary conditions. We discuss the critical crossover behavior of several observables, such as the magnetization and the correlation function of the longitudinal spin variables.

An effective characterization of the critical defect crossover is achieved by analyzing the ground-state fidelity, measuring the overlap between ground states associated with different defect parameters; cf. Eq. (16). Its associated susceptibility is proportional to the quantum Fisher information, which quantifies the reachable accuracy of the varying defect parameter. The fidelity provides information on the structure change of the ground state under variations of the defect, whether they give rise to substantial changes involving the whole system, or the changes remain limited to a finite region. In particular, within the critical crossover regime, the fidelity susceptibility diverges as a power L^ε, where $\varepsilon = 2y_\kappa = 7/4$ for bulk defects ($y_\kappa = 7/8$ is the RG dimension of the defect parameter) and $\varepsilon = 2y_\zeta = 1$ for boundary defects ($y_\zeta = 1/2$ is the RG dimension of the parameter associated with the boundary defects). On the other hand, the fidelity susceptibility remains finite, i.e., $O(1)$, outside the critical crossover region (where $|\kappa| \sim L^{-y_\kappa}$ or $|\zeta| \sim L^{-y_\zeta}$), i.e., for defects with finite strength. This means that a change of the defect strength, from $\kappa > 0$ to $\kappa + \delta\kappa$ with $\delta\kappa \ll 1$, causes only local changes of the ground state, unlike at $\kappa = 0$ where the changes involve the whole critical system, giving rise to the divergence of the fidelity susceptibility.

We have also presented numerical computations, obtained by exact diagonalization and DMRG, to support the theoretical FSS framework describing the critical crossover phenomena driven by symmetry-breaking defects at CQTs. They nicely confirm the scaling theory of the critical defect crossover.

It is worth noting that the critical crossover phenomena driven by symmetry-breaking defects are analogous to the critical crossovers between different fixed points of the bulk theory, arising from a relevant perturbation at an unstable fixed point, driving away the RG flow toward a stable fixed point (see, e.g., Refs. [8,53]).

The critical crossover phenomena driven by defects that we have discussed in this paper are quite general. Their emergence is expected to occur in generic models at CQTs in the presence of symmetry-breaking defects. Analogous phenomena are expected in the presence of $n > 1$ defects located in the bulk. Of course, for higher-dimensional systems another relevant factor concerns the spatial dimension of the defect, i.e., if it is localized at one point, along a line or within a surface. However, the RG arguments outlined here can be straightforwardly extended to allow for more complex

structures of defects in higher-dimensional quantum models. In this respect, one key feature is related to the value of the RG dimension of the corresponding defect parameter.

For example, one may consider the effect of one symmetry-breaking defect, such as that in Eq. (2), in the bulk of a two-dimensional quantum Ising model with symmetric boundary conditions, such as PBC or OBC. Then, one can analyze the corresponding RG perturbation (19) using the RG dimensions associated with the three-dimensional Ising universality class (see, e.g., Refs. [8,10] and references therein), obtaining a positive RG dimension y_κ for the defect parameter, $y_\kappa = z - y_\varphi = (z - \eta)/2 \approx 0.482$ (using $z = 1$ and $\eta \approx 0.036$). One then expect that one single symmetry-breaking defect in (strictly symmetric) two-dimensional quantum Ising system drives a critical crossover analogous to that found in quantum Ising rings, characterized by the divergence of the fidelity susceptibility associated with the defect (in this case we again expect $A_2 \sim L^{2y_\kappa}$ within the critical defect crossover, with $2y_\kappa \approx 0.964$).

Finally, the quantum-to-classical mapping [6,10] allows us to extend the quantum scaling scenarios to classical systems with one more spatial dimension and one more dimension of the defect. For example, a critical crossover scenario analogous to that driven by one symmetry-breaking defect in critical quantum Ising rings is expected to emerge in the case of a classical two-dimensional Ising systems defined in a slab with PBC and in the presence of a defect line that breaks the $\mathbb{Z}_2$ symmetry.

We conclude by mentioning that the scaling theory put forward in this paper, which describes the critical crossover behaviors driven by symmetry-breaking defects, can be verified with high accuracy in spin systems with a few dozen of qubits [as numerically done for chains of length $L \sim O(10)$]. It would be tempting to check our predictions in near-term experiments with quantum simulators operating on a limited amount of controllable qubits [54–56].

APPENDIX: DMRG COMPUTATIONS ON CHAINS WITH PBC

DMRG is commonly used with OBC rather than PBC, as the former allows us to obtain more accurate numerical results, a fact that is usually associated with the presence of entanglement entropy in the system at hand. Nevertheless, we used DMRG with PBC by enforcing the presence of the additional operator

$$-\hat{\sigma}_1^{(1)} \otimes \hat{\mathbb{1}} \otimes \cdots \otimes \hat{\mathbb{1}} \otimes \hat{\sigma}_L^{(1)} \qquad (A1)$$

into the superblock Hamiltonian.

We have implemented a combination of the standard two-site infinite-system and finite-system DMRG algorithms (respectively iDMRG and fDMRG) [57,58]. Before computing any observable in the fDMRG, the stability of the ground-state energy is verified within a discrepancy of 10^{-8} between two sequential lattice sweeps. We have also checked the stability of all our outcomes under increasing the bond dimension m of the blocks. Data for $\kappa = 1, 10$, at the quantum critical point, show small errors (smaller than the marker size, in all the plots presented in this paper) for a relatively small bond dimension $m = 15, 12$, for $L = 32$ and 40, respectively.

[1] K. G. Wilson, The renormalization group and critical phenomena, in *Nobel Lectures in Physics*, edited by Ekspöng, Vol. 6 (World Scientific, Singapore, 1993).

[2] M. E. Fisher, The renormalization group in the theory of critical behavior, Rev. Mod. Phys. **46**, 597 (1974).

[3] J. Zinn-Justin, *Quantum Field Theory and Critical Phenomena*, 4th ed. (Clarendon Press, Oxford, 2002).

[4] J. Cardy, *Scaling and Renormalization in Statistical Physics* (Cambridge University Press, Cambridge, 1996).

[5] S. L. Sondhi, S. M. Girvin, J. P. Carini, and D. Shahar, Continuous quantum phase transitions, Rev. Mod. Phys. **69**, 315 (1997).

[6] S. Sachdev, *Quantum Phase Transitions*, 2nd ed. (Cambridge University Press, Cambridge, 2011).

[7] P. Di Francesco, P. Mathieu, and D. Sénéchal, *Conformal Field Theory* (Springer-Verlag, New York, 1997).

[8] A. Pelissetto and E. Vicari, Critical phenomena and renormalization-group theory, Phys. Rep. **368**, 549 (2002).

[9] H. Nishimori and G. Ortiz, *Elements of Phase Transitions and Critical Phenomena* (Oxford University Press, Oxford, 2011), chap. 10.

[10] D. Rossini and E. Vicari, Coherent and dissipative dynamics at quantum phase transitions, Phys. Rep. **936**, 1 (2021).

[11] K. Binder, in *Critical Behavior at Surfaces*, edited by C. Domb and J. L. Lebowitz, Phase Transitions and Critical Phenomena Vol. 8 (Academic Press, London, 1983), p. 1.

[12] M. N. Barber, in *Finite-Size Scaling*, edited by C. Domb and J. L. Lebowitz, Phase Transitions and Critical Phenomena Vol. 8 (Academic Press, London, 1983), p. 145.

[13] H. W. Diehl, in *Field-Theoretic Approach to Critical Behavior at Surfaces*, edited by C. Domb and J. L. Lebowitz, Phase Transitions and Critical Phenomena Vol. 10 (Academic Press, London, 1986), p. 75.

[14] I. Affleck and A. W. W. Ludwig, Universal Noninteger 'Ground-State Degeneracy' in Critical Quantum Systems, Phys. Rev. Lett. **67**, 161 (1991).

[15] J. Cardy and D. C. Lewellen, Bulk and boundary operators in conformal field theory, Phys. Lett. B **259**, 274 (1991).

[16] R. Chatterjee and A. Zamolodchikov, Local magnetization in critical Ising model with boundary magnetic field, Mod. Phys. Lett. A **9**, 2227 (1994).

[17] E. Sela and A. K. Mitchell, Local magnetization in the boundary Ising chain at finite temperature, J. Stat. Mech. (2012) P04006.

[18] R. Z. Bariev, Effect of linear defects on the local magnetization of a plane Ising lattice, Zh. Eksp. Teor. Fiz. **77**, 1217 (1979) [Sov. Phys. JETP **50**, 613 (1979)].

[19] B. M. McCoy and J. H. H. Perk, Two-Spin Correlation Functions of an Ising Model with Continuous Exponents, Phys. Rev. Lett. **44**, 840 (1980).

[20] M. P. Nightingale and H. W. J. Blöte, Linear defects in two dimensional systems: A finite size investigation, J. Phys. A: Math. Gen **15**, L33 (1982).

[21] A. C. Brown, Critical properties of an altered Ising model, Phys. Rev. B **25**, 331 (1982).

[22] M. Oshikawa and I. Affleck, Defect Lines in the Ising Model and Boundary States on Orbifolds, Phys. Rev. Lett. **77**, 2604 (1996).

[23] M. Oshikawa and I. Affleck, Boundary conformal field theory approach to the critical two-dimensional Ising model with a defect line, Nucl. Phys. B **495**, 533 (1997).

[24] M.-C. Chung, M. Kaulke, I. Peschel, M. Pleimling, and W. Selke, Ising films with surface defects, Eur. Phys. J. B **18**, 655 (2000).

[25] D. Fichera, M. Mintchev, and E. Vicari, Quantum field theories and critical phenomena on defects, Nucl. Phys. B **720**, 307 (2005).

[26] V. Eisler and I. Peschel, Entanglement in fermionic chains with interface defects, Ann. Phys. (Berlin) **522**, 679 (2010).

[27] P. Calabrese, M. Mintchev, and E. Vicari, Entanglement entropy of quantum wire junctions, J. Phys. A **45**, 105206 (2012).

[28] G. Cuomo, Z. Komargodski, and M. Mezei, Localized magnetic field in the O(N) model, J. High Energ. Phys. 02 (2021) 134.

[29] V. Privman, editor, *Finite Size Scaling and Numerical Simulation of Statistical Systems* (World Scientific, Singapore, 1990).

[30] M. Campostrini, A. Pelissetto, and E. Vicari, Quantum transitions driven by one-bond defects in quantum Ising rings, Phys. Rev. E **91**, 042123 (2015).

[31] A. Pelissetto, D. Rossini, and E. Vicari, Out-of-equilibrium dynamics driven by localized time-dependent perturbations at quantum phase transitions, Phys. Rev. B **97**, 094414 (2018).

[32] M. Campostrini, A. Pelissetto, and E. Vicari, Quantum Ising chains with boundary fields, J. Stat. Mech. (2015) P11015.

[33] M. Campostrini, A. Pelissetto, and E. Vicari, Finite-size scaling at quantum transitions, Phys. Rev. B **89**, 094516 (2014).

[34] T. W. Burkhardt and I. Guim, Finite-size scaling of the quantum Ising chain with periodic, free, and antiperiodic boundary conditions, J. Phys. A: Math. Gen. **18**, L33 (1985).

[35] G. G. Cabrera and R. Jullien, Universality of Finite-Size Scaling: Role of the Boundary Conditions, Phys. Rev. Lett. **57**, 393 (1986); Role of the boundary conditions in the finite-size Ising model, Phys. Rev. B **35**, 7062 (1987).

[36] M. N. Barber and M. E. Cates, Effect of boundary conditions on the finite-size transverse Ising model, Phys. Rev. B **36**, 2024 (1987).

[37] L. Amico, R. Fazio, A. Osterloh, and V. Vedral, Entanglement in many-body systems, Rev. Mod. Phys. **80**, 517 (2008).

[38] S.-J. Gu, Fidelity approach to quantum phase transitions, Int. J. Mod. Phys. B **24**, 4371 (2010).

[39] D. Braun, G. Adesso, F. Benatti, R. Floreanini, U. Marzolino, M. W. Mitchell, and S. Pirandola, Quantum-enhanced measurements without entanglement, Rev. Mod. Phys. **90**, 035006 (2018).

[40] P. W. Anderson, Infrared Catastrophe in Fermi Gases with Local Scattering Potentials, Phys. Rev. Lett. **18**, 1049 (1967).

[41] S. L. Braunstein and C. M. Caves, Statistical Distance and the Geometry of Quantum States, Phys. Rev. Lett. **72**, 3439 (1994).

[42] M. G. A. Paris, Quantum estimation for quantum technology, Int. J. Quant. Inf. **7**, 125 (2009).

[43] P. Zanardi, M. G. A. Paris, and L. Campos Venuti, Quantum criticality as a resource for quantum estimation, Phys. Rev. A **78**, 042105 (2008).

[44] C. Invernizzi, M. Korbman, L. Campos Venuti, and M. G. A. Paris, Optimal quantum estimation in spin systems at criticality, Phys. Rev. A **78**, 042106 (2008).

[45] M. Campostrini, J. Nespolo, A. Pelissetto, and E. Vicari, Finite-Size Scaling at First-Order Quantum Transitions, Phys. Rev. Lett. **113**, 070402 (2014).

[46] A. Pelissetto, D. Rossini, and E. Vicari, Finite-size scaling at first-order quantum transitions when boundary conditions favor one of the two phases, Phys. Rev. E **98**, 032124 (2018).

[47] M. Caselle, M. Hasenbusch, A. Pelissetto, and E. Vicari, Irrelevant operators in the two-dimensional Ising model, J. Phys. A **35**, 4861 (2002).

[48] P. Calabrese, M. Caselle, A. Celi, A. Pelissetto, and E. Vicari, Nonanalyticity of the Callan-Symanzik β-function of two-dimensional O(N) models, J. Phys. A **33**, 8155 (2000).

[49] M. Campostrini, A. Pelissetto, P. Rossi, and E. Vicari, Two-point correlation function of three-dimensional O(N) models: The critical limit and anisotropy, Phys. Rev. E **57**, 184 (1998).

[50] M. Caselle and M. Hasenbusch, Critical amplitudes and mass spectrum of the 2D Ising model in a magnetic field, Nucl. Phys. B **579**, 667 (2000).

[51] D. Rossini and E. Vicari, Ground-state fidelity at first-order quantum transitions, Phys. Rev. E **98**, 062137 (2018).

[52] A_2 is computed by taking differences of the ground-state fidelity for κ and $\kappa + \delta\kappa$, with $\delta\kappa \ll 1$. The numeric second derivative is indeed computed with finite $\delta\kappa = 10^{-4}$, inverting Eq. (17). However, we checked the convergence for $\delta\kappa \to 0$, so that the corresponding relative error on the data, which is of the order of $\approx 10^{-4}$ for the point at the peak for $L = 20$, is always much smaller than the size of the symbols shown in Fig. 5.

[53] A. Pelissetto, P. Rossi, and E. Vicari, Crossover scaling from classical to nonclassical critical behavior, Phys. Rev. E **58**, 7146 (1998).

[54] J. Simon, W. S. Bakr, R. Ma, M. E. Tai, P. M. Preiss, and M. Greiner, Quantum simulation of antiferromagnetic spin chains in an optical lattice, Nature (London) **472**, 307 (2011).

[55] S. Debnath, N. M. Linke, C. Figgatt, K. A. Landsman, K. Wright, and C. Monroe, Demonstration of a small programmable quantum computer with atomic qubits, Nature (London) **536**, 63 (2016).

[56] A. Cervera-Lierta, Exact Ising model simulation on a quantum computer, Quantum **2**, 114 (2018).

[57] S. R. White, Density Matrix Formulation for Quantum Renormalization Groups, Phys. Rev. Lett. **69**, 2863 (1992).

[58] U. Schollwöck, The density-matrix renormalization group in the age of matrix product states, Ann. Phys. **326**, 96 (2011).